ACS OMEGA

Open Access

http://pubs.acs.org/journal/acsodf

Article

Graphene Quantum Dots Based on Mechanical Exfoliation Methods: A Simple and Eco-Friendly Technique

Zahra Azimi, Mahsa Alimohammadian, and Beheshteh Sohrabi*

Cite This: *ACS Omega* 2024, 9, 31427−31437

Read Online

ACCESS | Metrics & More | Article Recommendations | Supporting Information

ABSTRACT: Graphene quantum dots (GQDs) are very precious, widely used, and face significant challenges in preparation methods. In this study, three mechanical methods are investigated for the preparation of GQDs. All of these methods are green, cost-effective, and simple. In fact, Graphite, as a main source of GQDs, is exfoliated and fragmented under mechanical forces by sonication and ball milling. This mechanical exfoliation method is effective for converting large flakes of graphite into quantum dots. Additionally, the proposed methods are simple and faster than other top-down GQD fabrication methods. High-power sonication is applied to graphene flakes by using the liquid-phase exfoliation method. The liquid phase consists of ethanol and water, which are completely eco-friendly. Exfoliation and fragmentation of graphene flakes are performed using different sonication and ball-milling times. The obtained results from the analysis of the synthesized GQDs exhibit pristine graphene's distinct structural, chemical, and optical properties. Several analyses, such as X-ray diffraction (XRD) and Fourier transform infrared spectroscopy, were applied to study the product structure. Dynamic light scattering (DLS) and field emission scanning electron microscopy (FESEM) were used to examine product size and morphology, which confirmed the nanosize of GQDs. The smallest observed size of GQDs is approximately 23 nm. It is estimated that 95% of the nanoparticles are between 0.001 and 0.1 μm in size (41 nm). The optical properties of GQDs were investigated by using ultraviolet−visible and photoluminescence (PL) techniques. The PL peak wavelength is approximately 610 nm. Eventually, the results proved that the combined use of two methods, ultrasonication and ball milling during liquid-phase exfoliation, will be a simple, cheap, and suitable method for the production of GQDs.

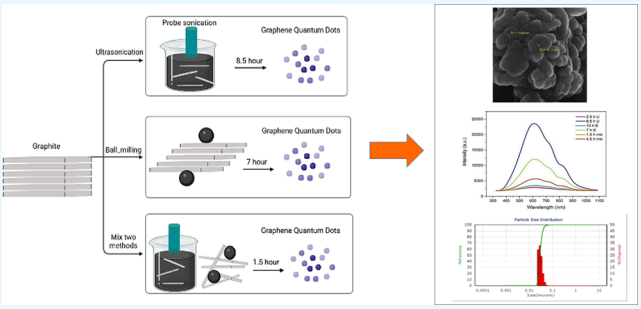

1. INTRODUCTION

Graphite has a layered structure. If graphene monolayers are placed on top of each other, a graphite structure is created.[1] Philip Wallace[2] first wrote about graphene in 1947, and since then, many efforts have been made to synthesize it easily. In 2004, two scientists from the University of Manchester were able to prepare this material with a simple method for the first time.[3] In other words, they showed that graphene can be experimentally prepared as the first two-dimensional material. Currently, graphene, with its unique properties, has become one of the subjects of discussion and research in the field of physics and material science. It is expected that this magical material can create a wide revolution in the manufacture of new electronic devices and be considered as a replacement for silicon in future electronics.[4,5] Graphene has revolutionized sensors[6,7] and energy storage[8,9] devices. In addition, graphene-based transistors[10] are also suitable for extreme temperatures and environments such as poles and space. When the dimensions of a material are continuously reduced from large to small scale, the properties of the material initially remain constant but gradually change as the dimensions approach the nano range (range between 1 and 100 nm).[11] One observation when the size of materials is reduced to the nanometer scale is the restriction on the motion of electrons due to the quantum confinement effect. This leads to the discretization of the electron energy level depending on the size of the material constraint. This obtained nanostructure shows remarkable electronic, physicochemical, mechanical, and magnetic properties not shown by large structures of the same material. Proper control over the dimensions and composition of such materials leads to profound features and responses commensurate with the development of new devices and technologies.[12,13] GQDs, which are small pieces (less than 100 nm) of graphene, have been developed in recent years.[14] In general, GQDs are 3−20 nm, and the thickness of their layers is 0.5−5 nm.[15] These nanomaterials are zero-dimensional, usually have a polycrystallized structure, and the single-crystalline type has good optical properties.[16] In contrast to graphene, these materials have

Received: January 14, 2024
Revised: June 9, 2024
Accepted: June 11, 2024
Published: July 12, 2024

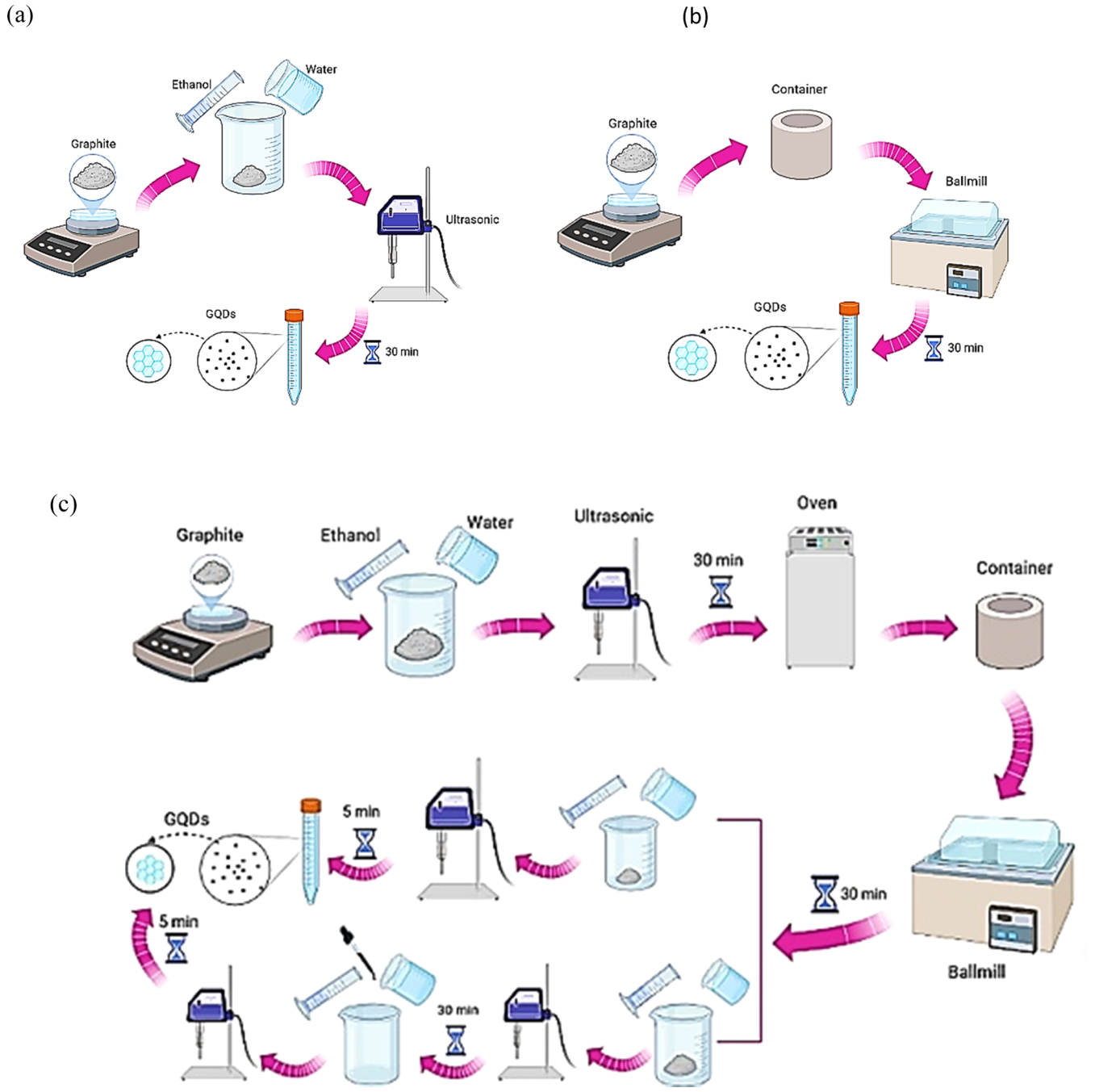

Figure 1. A schematic presenting the fabrication process of GQDs with (a) ultrasonic, (b) ball mill, and (c) combination of ultrasonic and ball mill.

band gaps, and theoretical calculations as well as optical and electrical experiments have shown the existence of this band gap in them.[17,18] Two factors called the edge effect and the quantum confinement effect are the basic characteristics of GQDs.[19] Moreover, the GQDs have better solubility than carbon nanotubes, which is due to their large edge effect, which can be modified by functional groups on their surface.[20] Unlike carbon nanotubes, which are limited to one-dimensional properties, GQDs are converted from two-dimensional graphene to zero-dimensional materials. This leads to quantum constraints and edge effects that significantly change the electron distribution due to the reduction of the crystal size to nanometers.[21] Their band gap energy can be adjusted by changing the size or chemical properties of the surface due to the quantum effect of the conjugate π spheres and the edge effect.[22,23] Until now, different synthesis methods for GQDs have been investigated.[24,25] There are many restrictions, such as complex synthesis methods, high cost, toxic materials such as strong acids or oxidants, and expensive tools that may damage the main structure of the graphitic source and produce many defects and functional groups on the GQD's surface. As a result, it is important to develop a simple, green, and economical route for the synthesis of GQDs. Liquid-phase exfoliation is often one of the most convenient methods in GQD production.[26] This approach has been used for a large range of layered materials, including graphene. It applies ultrasound[27] or high shear force[28] to layered materials in suitable solvents for the production of nanosheets and

https://doi.org/10.1021/acsomega.4c00453
ACS Omega 2024, 9, 31427−31437

quantum dots. The simplest way to disperse graphite is with the appropriate solvents. After the layers are removed, if steric and electronic factors are allowed to penetrate, the solvent molecules can be placed between the layers. Depending on the ability of the solvents to stabilize the sheets, the exfoliated materials may be stable or aggregated. If great stabilization is obtained from the interaction between the material and the solvent, then the stability of the dispersed state after exfoliation is good. Therefore, it is important to choose a suitable solvent that maintains the dispersed state of suspension and prevents reaggregation during liquid-phase exfoliation. For most solvents, dispersion using ultrasound is rapidly followed by aggregation and sedimentation. Until now, many main organic solvents (NMP, DMF, GBL, DMEU, IPA, and THF) have been used for graphene exfoliation.[29−31] Research has demonstrated that the liquid surface tension is the most significant factor in graphene dispersion. The basis of this approach is to modify the surface tension of the liquid near the energy between the graphite layers. The energy between the graphite layers is estimated to be around 40 mN m^{-1}. As a result, solvents such as water and ethanol[32] with a surface tension of 72 and 23 mN m^{-1}, respectively, are incapable of dispersing graphene alone. Thus, when using solvents, a mixture of them should be applied. By combining a certain percentage of these solvents, the surface tension of the liquid phase can be adjusted between 40 and 50 mN m^{-1}. Similar to the ultrasound method, the high energy of ball milling has also shown the ability to exfoliate layered materials such as graphene into nanosheets and quantum dots in the liquid phase.[33] Until now, many research groups have tried to prepare graphene nanosheets and quantum dots using the ball mill[31,34−41] and ultrasound methods.[42−46]

Herein, green, low-cost, and simple methods for preparation and dispersion of such GQDs in the liquid phase are represented. This approach is achieved by mechanically exfoliating graphite in an ethanol/water mixture and forming a stable dispersion of monolayer and few-layer GQDs. It is well known that the long reaction time associated with oxidative cleavage and hydrothermal/solvothermal methods is one of the most common problems. Conversely, the ultrasonic-assisted technique is widely used to prepare GQDs by a rapid method. As a result of ultrasonic waves, many small bubbles form in the liquid phase. These bubbles create high pressure and energy. As they grow and collapse, the C−C bonds are destroyed. Besides, it can reduce reaction time and improve production yield. These ultrasonic-assisted methods avoid the conventional use of strong oxidants and surfactants; therefore, the graphitic structure is well maintained without destruction. Moreover, benefiting from the use of ethanol and water, it does not need any special post-treatment to remove the impurity, which could be great for potential applications in electronic, optical, and energy areas.

2. EXPERIMENT

2.1. Materials. The graphite powder (Product No. 332461) and ethanol (99%) used in all experiments were purchased from Merck. Deionized water was used throughout the experiments.

2.2. Procedure. Generally, for the preparation of GQDs, ultrasonic and ball-milling techniques were used. GQDs were prepared by three different methods: ultrasonic, ball mill, and a mixture of both. An attempt was made to produce quantum nanoparticles by using three different methods. Each method is described below.

2.2.1. Preparation of GQDs Using Ultrasonic. As illustrated in Figure 1a, 1.25 g of pure graphite was initially added to 250 mL of ethanol/water combination in a 20:80 ratio. The resultant black suspension was subjected to ultrasonic waves of the greatest strength (400 W) for 10 h in order to create flaked graphite, graphene layers, and quantum dots. Every 30 min, 0.5 mL of the suspension was collected and mixed with 50 mL of a 20:80 ethanol/water combination. Sampling was carried out in order to collect data for analysis.

2.2.2. Preparation of GQDs Using Ball Mill. As shown in Figure 1b, 1.25 g of pure graphite was poured into a 20 mL container. Then two small steel balls were used to exfoliate the material inside the container. The rotation speed was controlled at 20 Hz. The graphite was subjected to the shearing force of the mill at medium speed for 10 h. Every 30 min, 0.0025 g of the ball mill powder was picked up and added to 50 mL of a 20:80 ethanol/water mixture. The dispersed sample was kept for analysis.

2.2.3. Preparation of GQDs Using a Combination of Ultrasonic and Ball Mill. This method employs both ultrasonic waves and a ball mill. As shown in Figure 1c, initially, 1.25 g of pure graphite is added to 250 mL of ethanol/water mixture in a ratio of 20:80. After stirring, the resulting black suspension is exposed to ultrasonic waves with a power of 400 W for 30 min. The resulting suspension is then dried in an oven at 70 °C for 15 h. After collecting, the resulting powder is added into the mill container and placed under the shearing force of the ball mill at 20 Hz speed for 30 min. The dispersed suspension is then added to 50 cc of ethanol/water combination in a 20:80 ratio for 5 min under ultrasonic waves with maximum power (400 W). This process is repeated for 10 h, and the samples are collected for analysis.

2.3. Characterization. UV−vis spectra were recorded by using quartz cuvettes with an optical path length of 1 cm on a Shimadzu 2550 (220 V) spectrophotometer at wavelengths ranging from 200 to 400 nm. A Philips PW1480 diffractometer was used to collect X-ray diffraction (XRD) patterns (Cu Kα radiation). The scanning electron microscopy (SEM) investigations were carried out with the aid of a field emission scanning electron microscope (FESEM, Tescan Vega3) with a 20 kV acceleration voltage. The samples were sputtered with gold before SEM analysis. A Raman spectrometer (Firstguard) equipped with a 532 nm laser excitation was used to record spectra in the wavenumber range of 0−4000 cm^{-1}. Fourier transform infrared (FTIR) spectra were collected with a (PerkinElmer 1720-x) FTIR spectrophotometer by using the KBr pellet method. DLS analysis was performed using a Nanoflex 180.

3. RESULTS AND DISCUSSION

3.1. UV−Vis Absorption Analysis. UV−vis spectroscopy is the most fundamental method for characterizing colloidal dispersions. This analysis can provide information about the structure of the quantum dots. GQDs show a broad absorption peak in the ultraviolet−visible range. The UV−vis spectrum of GQDs includes two absorption peaks. The peak at 250−280 nm was related to the $\pi \rightarrow \pi^*$ band of sp^2 carbons in the aromatic structure of GQDs.[47] Moreover, the peak found in the 310−370 nm wavelength region could be related to $n \rightarrow \pi^*$ transitions, originating from C═O bonds (COOH groups). The absorption intensity may be used to calculate the

https://doi.org/10.1021/acsomega.4c00453
ACS Omega 2024, 9, 31427−31437

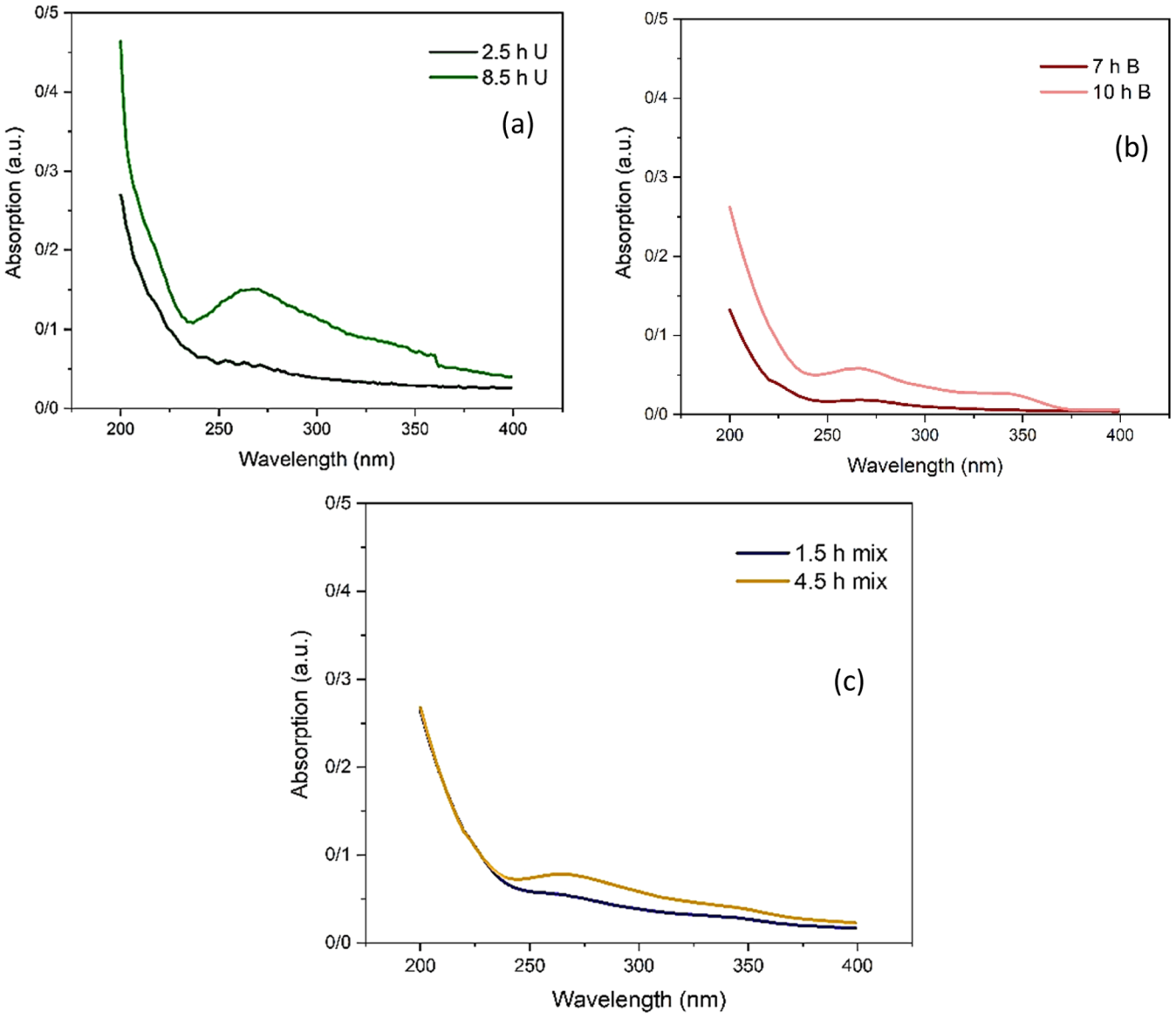

Figure 2. UV−Vis absorption spectra of GQDs produced from three exfoliation techniques: (a) ultrasonication (400 W, 2.5 h, 8.5 h), (b) ball mill (7, 10 h), (c) combination of ultrasonication and ball mill (1.5, 4.5 h).

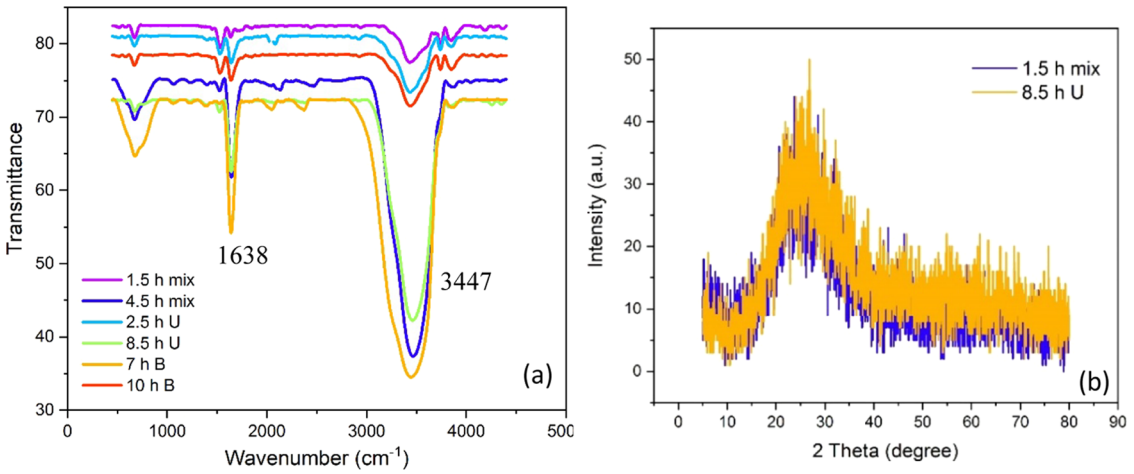

Figure 3. (a) Infrared spectrum of optimal samples of GQDs (up) and (b) XRD patterns of ultrasonication sample (8.5 h) and combination of ultrasonication and ball mill (1.5 h) (down).

https://doi.org/10.1021/acsomega.4c00453
ACS Omega 2024, 9, 31427−31437

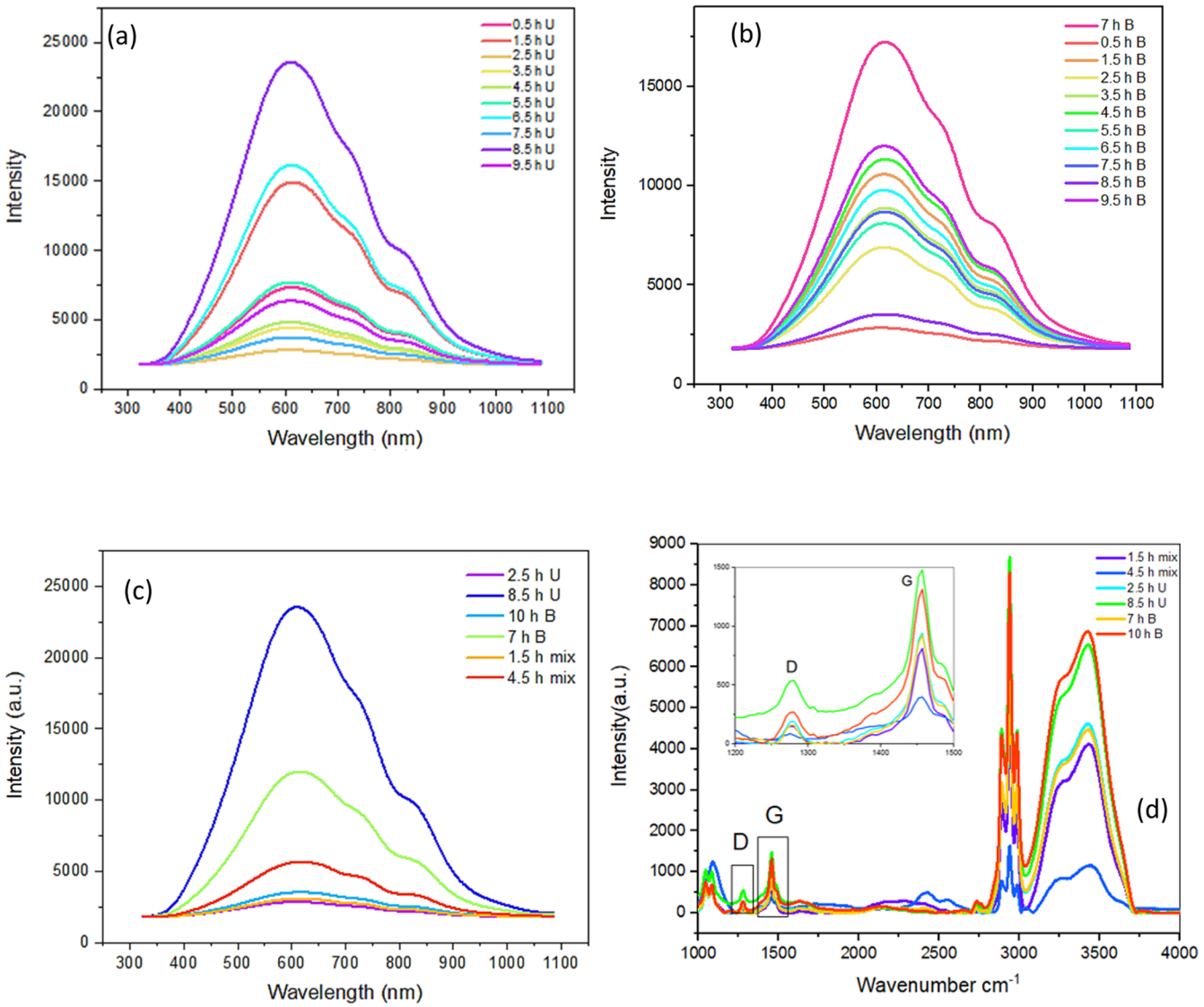

Figure 4. Diagram related to the fluorescence spectrum of (a) ultrasonication, (b) ball mill, (c) optimal samples of GQDs, and (d) Raman spectrum of samples of GQDs (zoomed D and G peak in the inset).

concentrations of these nanoparticles in the solution. Examining the results reveals one peak in the UV spectra of these nanomaterials. In this work, a peak at 270 nm is related to the $\pi \rightarrow \pi^*$ transition of aromatic ring C═C bonds. In addition, the disappearance of the n-π^* peak can be shown in the synthesized samples, which is related to the absence of oxygenated functional groups. It was observed that with the increase in the number of quantum dots, the intensity of the absorption peak also increases. The absorption spectra of optimum samples containing GQDs generated utilizing three exfoliation processes (ultrasound, ball mill, and a combination of both) are shown in Figure 2a–c. This figure depicts a graph showing the amount of absorption of all GQDs generated by ultrasound at various periods (Figure 2a). The absorption peak of all samples was seen at 270 nm due to the transition between the $\pi \rightarrow \pi^*$ bands, indicating that graphene in the ethanol/water solution has no perturbation in the electrical structure. This performance is compatible with the absorption spectra of the GQDs reported results. Furthermore, the lack of the absorption peak at 229 nm, which is associated with graphene oxide, verifies the absence of graphene oxide in the samples.[48] We concluded that the optimal samples (8.5 h of ultrasound, 10 h of ball milling, and 4.5 h of the combination of ultrasound and ball milling) obtained the most quantum dots and showed the highest absorption in the ultraviolet spectrum after examining the results and comparing the graphs of the three exfoliation methods (Figure 2b,c).

3.2. FTIR Analysis of GQD Samples. IR spectroscopy, which is a rapid and straightforward approach for studying the chemical functional groups contained in synthesized GQDs, is the second most frequent technique for the characterization of GQDs. There should be no peaks in the spectra of pure graphite and graphene due to the lack of particular functional groups. Peaks in the infrared spectra of graphite and graphene are commonly observed due to the absorption of solvent molecules and moisture. According to Figure 3a, the strongest peak of the GQD spectra is situated at around 3447 cm^{-1} and may be attributed to the stretching vibrations of hydroxyl (O–H) groups. Considering that the test was conducted in liquid phase, this peak is extremely intense. The occurrence of (C═C) bond vibration at 1638 cm^{-1} in the FTIR spectra of GQDs is connected to the honeycomb structure of graphene.

https://doi.org/10.1021/acsomega.4c00453
ACS Omega 2024, 9, 31427–31437

Exfoliated graphite has a rather significant peak at around 670 cm^{-1}, which is associated with aromatic compounds (C−H). As evidenced by the IR spectra, it is inferred that no chemical functional groups exist in the produced GQDs.

3.3. XRD Pattern. An XRD pattern can be used to investigate the crystal structures of GQDs. Figure 3b depicts the resulting XRD patterns of the synthesized GQDs. Harsh sonication and ball milling were used to prepare these samples (1.5 h mix and 8.5 h u). In these two samples, the sharp peak of the (002) basal planes in graphite has mostly vanished. These nanoparticles' diffraction peaks are like those of primary graphite (Figure S1), indicating that their crystalline structure is preserved after exfoliation. Because of the reduction in the crystal size and layer thickness, the diffraction peaks of GQDs are wider than those of graphite. GQDs have a fairly broad peak around $2\theta = 25°$. Graphite's X-ray diffraction pattern also shows a sharp peak at 26°. The peak width at half the maximum height has an inverse relationship with the grain size, according to the Scherrer equation ($L = K\lambda/\beta\cdot\cos\theta$).[49] In this equation, λ is the X-ray wavelength, is the peak width at half the maximum height (should be replaced in radians), θ is the peak diffraction angle, and L is the crystallite size. K is a constant that varies with crystallite shape and is usually taken to be 0.9. As the grain size decreases, the width of the peak increases, and its intensity decreases. As a result, the peaks of the nanoparticles are easily distinguished from the raw materials. It should be noted that the broadening of the peaks is affected by other factors such as the presence of stress in the sample, machine error, and X-ray nonuniformity, and all possible factors are considered when interpreting the results. The crystal size of the synthesized GQDs is approximately 20 nm, according to this equation.

3.4. Photoluminescence Analysis. GQDs exhibit an excitation-dependent photoluminescence (PL) activity. GQD fluorescence is affected by the size and the preparation method.[48,50] When external energy is applied to GQDs, they emit light, which can be precisely adjusted to produce a variety of colors as a result of a change in the GQDs' size. As an electron transitions from the maximum valence band to the minimum conduction band, a band edge emission occurs. On the other hand, phonon-assisted emission occurs when an electron loses energy to a phonon before relaxing to the ground state. Changing the band gap based on GQD size is especially important for solar cell applications.[51] The band gap of GDQs is essentially determined by the size, shape, and number of sp^2−sp^3 hybridized domains in them. Figure 4a,b compares the photoluminescence (PL) spectra of GQDs synthesized by using various techniques and at different times. The highest occupied molecular orbital and the lowest unoccupied molecular orbital play essential roles in the PL properties of a compound. This electronic transfer may be related to the n-orbitals of oxygen atoms in GQDs, that is, the electrons in their n-orbitals are excited by light and transferred to the π^* orbitals of the graphitic structure of quantum dots. As shown in Figure 4a,b, the fluorescence spectra of all samples of graphene quantum dots prepared by ultrasound and ball mill are shown. A maximum emission of 610 nm was observed at 8.5 h, which corresponded to the optimal sample. In addition, the maximum emission in ball mill spectrum occurs at 614 nm, which corresponds to an optimal sample (7 h). Figure 4c shows the fluorescence spectrum of the optimal samples of GQDs. The emission spectrum has a sharp peak at 610 nm and a shoulder at 830 nm. This double-peak photoluminescence is common in polyaromatic structures.[52] The formation of the intrinsic state in GQDs is attributed to the red emission and a strong absorption peak on the higher energy level observed in this study.

3.5. Raman Spectroscopic Analysis. Raman spectroscopy, which suggests an individual fingerprint of the lattice vibrations and crystalline structure, was also widely used in this study. This analysis looks at the number of structural defects as well as the quality of the quantum dots. For graphite as the source, three bands have been identified: D, G, and 2D.[53] The amount is represented by the ratio of the intensity of the D band to the intensity of the G band (I_D/I_G). The D peak in 2D carbon structures is observed due to a lack of order in these structures. The G peak is caused by the stretching of the C−C bond in graphite structures.[54] The degree of structural disorder in graphene sheets can be estimated by the intensity ratio (I_D/I_G). The smaller the I_D/I_G value, the better the crystal quality of the structure.[55] As evidence, the Raman spectrum was extracted from the original graphite powder (Figure S2) and then compared with the GQDs. From the optimal samples prepared by all three methods, which included GQDs with the smallest size, the Raman spectrum was taken, and the results are presented in Figure 4d. Hydrogen bonding plays a substantial part in forming the structure of water−ethanol solutions. The behavior of the OH stretching band in water−ethanol solutions is essentially influenced by hydrogen bonding. In the water−ethanol system, the extremely wide broad band of OH-groups of water−ethanol molecules extends from 2900 to 3800 cm^{-1}. In the region 2800−3000 cm^{-1}, the stretching lines of CH-groups overlap with a wide band of OH-groups.[56]

Peak D in the 2.5 and 8.5 h ultrasound samples is located at 1280 cm^{-1}, indicating carbon atom vibrations with sp^3 hybrid, whereas G peak at 1457 cm^{-1} is related to carbon atom vibrations with sp^2 hybrid. The relative intensities (I_D/I_G) in the 2.5 and 8.5 h samples are 0.181 and 0.65, respectively, indicating that GQDs have a regular structure similar to graphite. Peak D at 1281 cm^{-1} and peak G at 1457 cm^{-1} in samples ball milled for 7 and 10 h are shown in Figure S3b. The relative intensity of the D and G peaks (I_D/I_G) is 0.2 in the 7 h sample and 0.36 in the 10 h sample. Figure S3c shows that in samples of 1.5 and 4.5 h resulting from the combination of ultrasonic and ball milling methods, peaks D and G are observed at 1280 and 1457 cm^{-1}, respectively. The relative intensity of peak D and G (I_D/I_G) in the sample of 1.5 h is equal to 0.17, and in the sample of 4.5 h, it is equal to 0.20. According to the Raman results, it is concluded that the intensity of all of the spectra D bands is significantly higher than that of the initial graphite powder, which indicates the creation of defects during the process of preparing GQDs. We can divide such defects into two main types: plane defects, such as point defects on the base plane, and edge defects. Because ultrasonic waves cut the original large plates into smaller pieces, edge defects are unavoidable during the processing process. The number of edge defects increases because these smaller pieces have more edges per unit mass. Raman spectroscopy, on the other hand, determined that long-term ball milling and ultrasonic-based exfoliation cause a high degree of defect. Despite the high efficiency of high-power ultrasound in preparing quantum dots, one of its weaknesses is the presence of defects and the small lateral size of the final products.

https://doi.org/10.1021/acsomega.4c00453
ACS Omega 2024, 9, 31427−31437

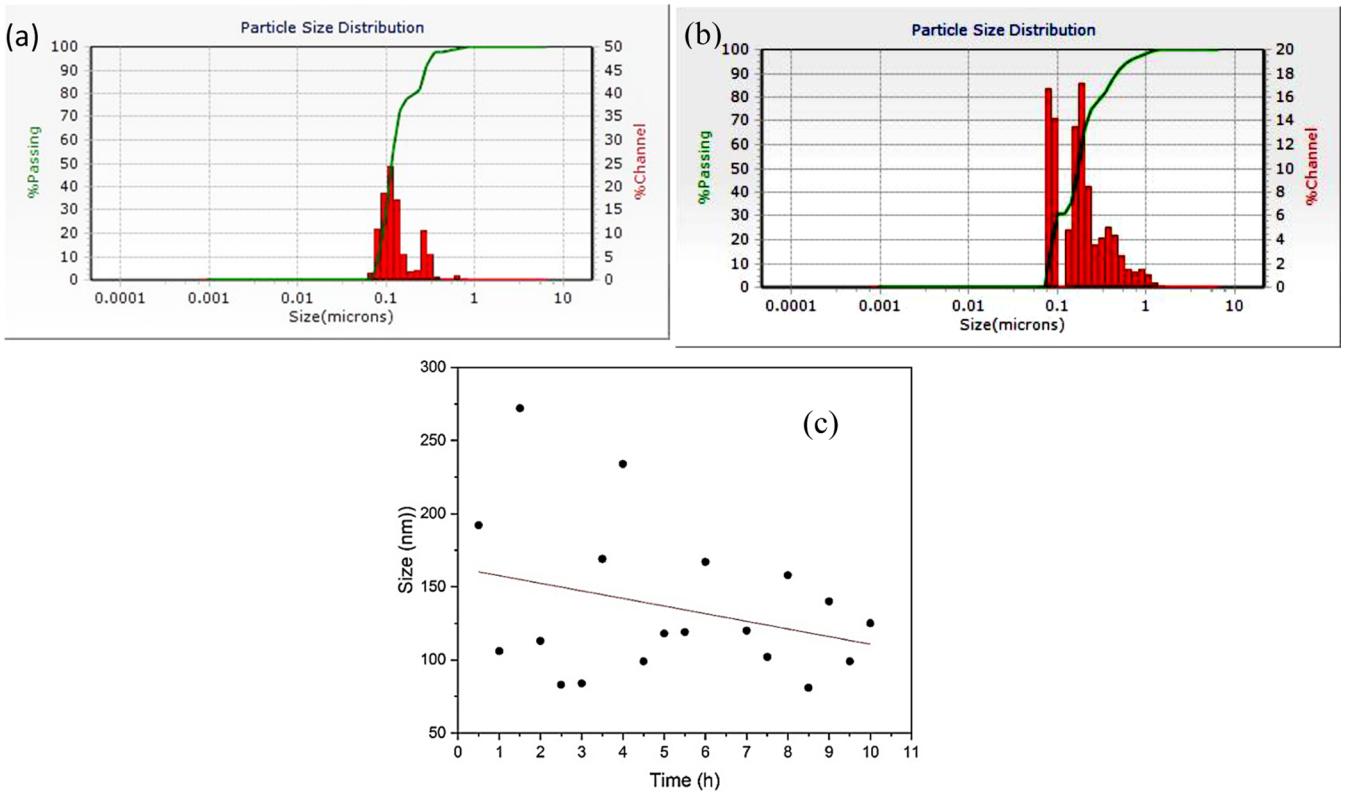

Figure 5. Particle size distribution diagram (a) after 2.5 h, (b) after 8.5 h of ultrasonication, and (c) of all samples after 10 h ultrasonication.

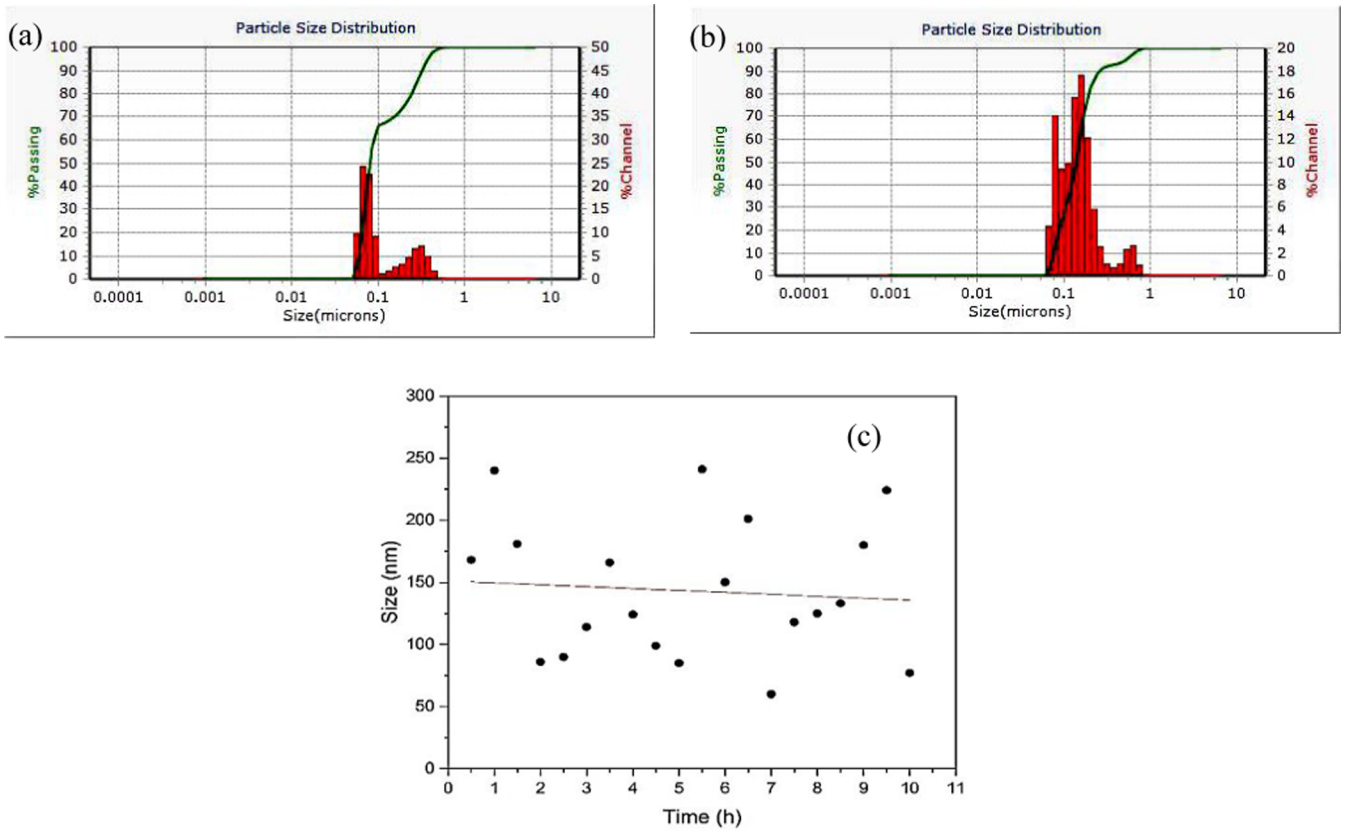

Figure 6. Particle size distribution diagram (a) after 7 h, (b) after 10 h of ball mill, and (c) of all samples after 10 h of ball mill.

3.6. DLS Analysis. Figures 5−7 show the results of the DLS analysis. The size distribution graphs of the synthesized GQDs with ultrasonication, ball milling, and combination methods are observed. The particle size distribution of optimal

https://doi.org/10.1021/acsomega.4c00453
ACS Omega 2024, 9, 31427−31437

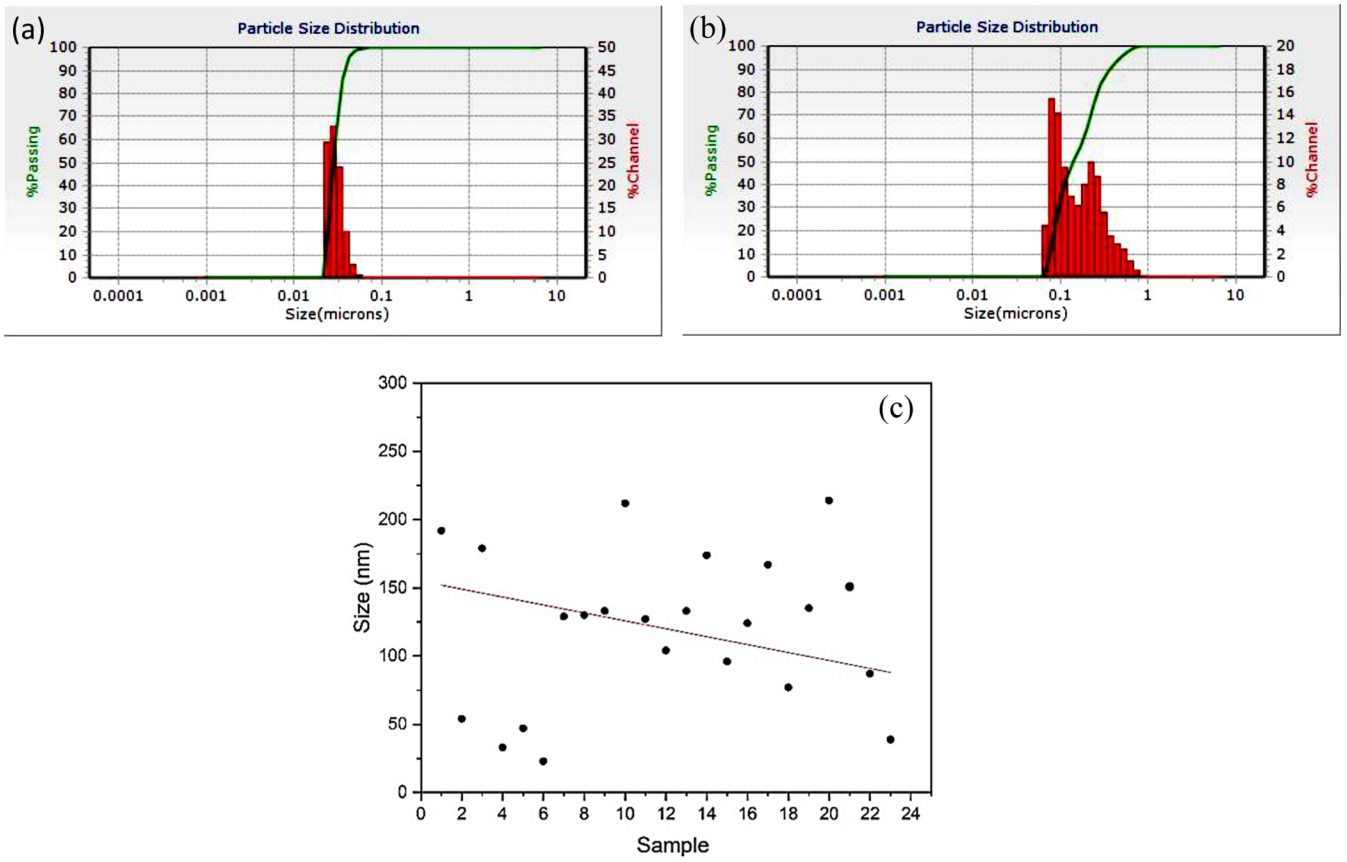

Figure 7. Particle size distribution diagram (a) after 1.5 h and (b) after 4.5 h of combination method of ultrasonic and ball mill (c) of all samples after use of both exfoliation methods (ultrasonic and ball mill).

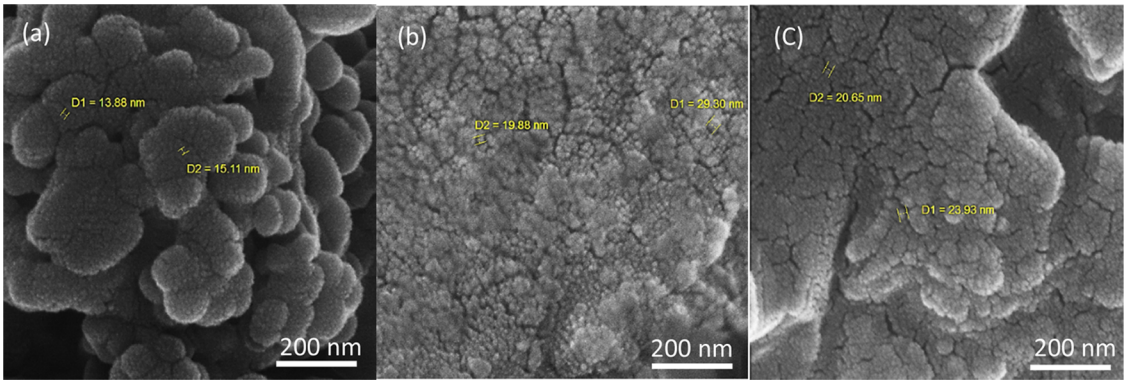

Figure 8. (a–c). FESEM images related to the sample of (a) ultrasonication of sample for 2.5 h, (b) ball milling of sample for 7 h, and (c) combination of ultrasonic and ball milling at high magnification for 1.5 h.

samples (2.5 and 8.5 h) using the ultrasonic method is depicted in Figure 5a,b. The valuation of the results shows that after 2.5 h of ultrasonication, the size of quantum dots reaches 83 nm, and %95 of the particles have dimensions between 0.1–1 μm. As the exfoliation process continued, after more than 8 h, the number of particles with sizes of about 0.1 μm increased noticeably. To better investigate the exfoliation process with the ultrasound method, the time–size graph for all samples was drawn during the DLS measurement (Figure 5c). For more details, Figure S4 is provided in the Supporting Information.

Figure 6a,b depicts the particle size distribution of optimal samples (7 and 10 h) prepared using the ball mill method. The graphs show that after 7 h of using the ball mill machine, a few GQDs reach a size of about 60 nm, and 95% of them reach a size of about 365 nm. The size of more quantum dots gradually decreases as the ball-milling time increases. The time–size graph for all samples was drawn during the DLS measurement to better investigate the exfoliation process using the ball mill method (Figure 6c). For more details, Figure S5 is provided in the Supporting Information.

Figure 7a,b depicts the particle size distribution using a combination of ultrasonic and ball mill methods. The graphs show that the quantum dots reach their smallest size, which is 23 nm. In this case, 95% of the particles have dimensions ranging from 0.001–0.1 μm (about 41 nm). The particle size

https://doi.org/10.1021/acsomega.4c00453
ACS Omega 2024, 9, 31427–31437

changes when the time is increased to 4.5 h, and approximately 95% of them are between 0.1 and 1 μm. It can be seen that the graphene particles are very small in the early hours, and in fact, using both methods for exfoliation increases the efficiency and speed of the final production. The particle size distribution of GQDs (Figure 7a) showed that the synthesized GQDs had a polydispersity index (PDI) of 0.43. As the exfoliation time increases, the GQDs aggregate to form large particles. The particle size distribution of the 4.5 h sample with a PDI equal to 0.82 (Figure 7b) proves the formation of aggregates. In other words, this PDI value indicates a very broad particle size distribution. To better investigate the exfoliation process by the combined ultrasonic and ball-milling methods, the time−size diagram for all samples during the DLS measurement is also drawn (Figure 7c). For more details, Figure S6 is provided in the Supporting Information.

3.7. FESEM Images. Figure 8a−c shows FESEM images of GQDs at various scales and times. Due to the difference in the preparation of samples and the use of two methods, ball mills and ultrasound, the images of the particles are different. Due to the flexible structure of graphene, folds and wrinkles are created in its structure as a result of the pressure that comes from the balls of the grinding machine and the ultrasonic waves. A ball mill can destroy the aggregate state of graphene powder to create a multilayered state. The structure of the obtained graphene was investigated to clarify the effect of ball milling and ultrasound. The thickness of all graphene samples decreased, indicating graphite exfoliation to graphene. GQDs have a spherical structure, and the boundary between the particles is well defined. The SEM images show that the GQDs are initially produced, and then the produced nanoparticles are quickly adhered together again and thus accumulate due to the high energy produced during ultrasound and ball milling. The defect of graphite plates can be attributed to ultrasound waves using the method of preparing quantum dots by ultrasound. Waves are generated in this method by the collapse of bubbles in the liquid, which causes a local increase in the pressure and temperature. The waves travel from the solvent to the liquid−solid interface, where they can be converted to sound waves in graphite. Figure 8a shows a FESEM image of GQDs prepared by the ultrasound method at high magnification. As can be seen in this image, the uniformity of the size of the quantum particles is greater than that with the previous method. The lower amount of energy given in the exfoliation operation with the help of ultrasound waves in less time (2.5 h) probably caused more uniformity of the particles, so that the gaps between the spheres when using both an ultrasonic device and a ball mill are not seen here. Figure 8b shows a high-magnification FESEM image of GQDs prepared by the ball-milling method. As can be seen in this image, it is not possible to distinguish the exact boundary between the particles, which is probably due to the energy and pressure that are created during the long period of time used in the ball mill machine. Figure 8c shows an FESEM image of GQD nanoparticles prepared by combining ultrasound and ball-milling methods at high magnification. As it is clear in the images, it is impossible to distinguish the exact boundary between the particles. In fact, the high temperature and pressure that occur during the preparation of quantum dots, both through ultrasound waves and during crushing due to the impact and friction of the balls in the ball mill machine, can cause the accumulation of these nanoparticles. Figures S7−S9 provide additional information. Agglomeration of particles was observed in samples, which has two reasons; one of them is magnetization attraction between particles. Based on our previous studies,[57,58] pressure has changed the electronic structure of graphene and led to inducing magnetism inside graphene flakes. In these methods, pressure from the mechanical forces could lead to weak magnetization that increases the attraction between the particles and also increases the agglomeration, and the other reason is the time gap between sample preparation and their imaging records by FESEM, which has several days. During this time, particles have reaggregated to each other, leading to an increased level of agglomeration, despite the application of ultrasonics during sample preparation.

4. CONCLUSIONS

In summary, we report cost-effective, environmentally friendly methods for producing graphene quantum dots (GQDs) using graphite as the carbon precursor. GQDs require exfoliation of the carbon source to achieve quantum dots in the liquid phase. Three methods are used for the preparation of GQDs based on mechanical exfoliation techniques in two solvents, water and ethanol, resulting in GQD-U, GQD-B, and GQD-Mix. Graphite was easily exfoliated in low-boiling-point solvents without the use of a surfactant. In addition, water offers benefits as a solvent: being economical, abundant, and nontoxic. The appropriate method and the most optimal time for preparing GQDs were determined. Exfoliation benefits and efficiency can be increased by combining the methods, resulting in a faster and more efficient process. The graphs show that GQD-Mix has the smallest size at 23 nm. It is estimated that 95% of the nanoparticles are between 0.001 and 0.1 μm in size (41 nm). Additionally, the relative intensity of peak D and G (I_D/I_G) in the sample of 1.5 h combination of both ultrasonication and ball milling is equal to 0.17. Also, these nanoparticles show excellent photoluminescence properties. The research on GQD is still in its early stages, yet the number of applications for this material keeps rising. It is hoped that this article will be a helpful resource for chemists working on the design and production of advanced GQD materials and products.

■ ASSOCIATED CONTENT

Supporting Information

The Supporting Information is available free of charge at https://pubs.acs.org/doi/10.1021/acsomega.4c00453.

XRD pattern of graphite (Figure S1), Raman spectrum of graphite (Figure S2), Raman spectrum of GQDs prepared by ultrasonic, ball mill, and the combination method of ultrasonic and ball mill (Figure S3), particle size distribution diagram after 4 h, after 6 h, and after 10 h of ultrasonication (Figure S4), particle size distribution diagram after 1 h, after 3 h of ball mill, and after 5 h of ball mill (Figure S5), particle size distribution diagram after 0.5 h, after 3 h, and after 6 h of the combination method of ultrasonic and ball mill (Figure S6), FESEM images related to the sample of 2.5 h of ultrasonic low magnification and high magnification (Figure S7), FESEM images related to the sample of 7 h of ball mill, low magnification, and high magnification (Figure S8), and FESEM images related to the sample of 1.5 h of combination of ultrasonic and ball-milling low magnification, high magnification (Figure S9) (PDF)

https://doi.org/10.1021/acsomega.4c00453
ACS Omega 2024, 9, 31427−31437

AUTHOR INFORMATION

Corresponding Author

Beheshteh Sohrabi − *Surface Chemistry Research Laboratory, Department of Chemistry, Iran University of Science and Technology, P.O. Box 16846-13114 Tehran, Iran;* orcid.org/0000-0001-9091-6255; Phone: +982173228315; Email: Sohrabi_b@iust.ac.ir, Sohrabi_b@yahoo.com; Fax: +982177491204

Authors

Zahra Azimi − *Surface Chemistry Research Laboratory, Department of Chemistry, Iran University of Science and Technology, P.O. Box 16846-13114 Tehran, Iran*

Mahsa Alimohammadian − *Surface Chemistry Research Laboratory, Department of Chemistry, Iran University of Science and Technology, P.O. Box 16846-13114 Tehran, Iran*

Complete contact information is available at: https://pubs.acs.org/10.1021/acsomega.4c00453

Notes

The authors declare no competing financial interest.

ACKNOWLEDGMENTS

The Iran University of Science and Technology has supported this work greatly. Therefore, the authors want to thank them absolutely for all of their help.

REFERENCES

(1) Katsnelson, M. I. Graphene: Carbon in Two Dimensions. *Mater. Today* **2007**, *10* (1−2), 20−27.

(2) Wallace, P. R. The Band Theory of Graphite. *Phys. Rev.* **1947**, *71* (9), 622−634.

(3) Novoselov, K. S.; Geim, A. K.; Morozov, S. V.; Jiang, D.; Zhang, Y.; Dubonos, S. V.; Grigorieva, I. V.; Firsov, A. A. Electric Field Effect in Atomically Thin Carbon Films. *Science* **2004**, *306* (5696), 666−669.

(4) Cooper, D. R.; D'Anjou, B.; Ghattamaneni, N.; Harack, B.; Hilke, M.; Horth, A.; Majlis, N.; Massicotte, M.; Vandsburger, L.; Whiteway, E.; Yu, V. Experimental Review of Graphene. *ISRN Condens. Matter Phys.* **2012**, *2012*, 501686.

(5) Si, C.; Sun, Z.; Liu, F. Strain Engineering of Graphene: A Review. *Nanoscale* **2016**, *8* (6), 3207−3217.

(6) Justino, C. I. L.; Gomes, A. R.; Freitas, A. C.; Duarte, A. C.; Rocha-Santos, T. A. P. Graphene Based Sensors and Biosensors. *TrAC, Trends Anal. Chem.* **2017**, *91*, 53−66.

(7) Yavari, F.; Koratkar, N. Graphene-Based Chemical Sensors. *J. Phys. Chem. Lett.* **2012**, *3* (13), 1746−1753.

(8) Olabi, A. G.; Abdelkareem, M. A.; Wilberforce, T.; Sayed, E. T. Application of Graphene in Energy Storage Device−A Review. *Renewable Sustainable Energy Rev.* **2021**, *135*, No. 110026.

(9) Tiwari, J. N.; Tiwari, R. N.; Kim, K. S. Zero-Dimensional, One-Dimensional, Two-Dimensional and Three-Dimensional Nanostructured Materials for Advanced Electrochemical Energy Devices. *Prog. Mater. Sci.* **2012**, *57* (4), 724−803.

(10) Sharma, B. K.; Ahn, J. H. Graphene Based Field Effect Transistors: Efforts Made towards Flexible Electronics. *Solid State Electron.* **2013**, *89*, 177−188.

(11) Sumanth Kumar, D.; Jai Kumar, B.; Mahesh, H. M.Quantum Nanostructures (QDs): An Overview. In *Synthesis of Inorganic Nanomaterials: Advances and Key Technologies*; Elsevier, 2018; pp 59−88.

(12) Efros, A. L.; Brus, L. E. Nanocrystal Quantum Dots: From Discovery to Modern Development. *ACS Nano* **2021**, *15* (4), 6192−6210.

(13) Ghaffarkhah, A.; Hosseini, E.; Kamkar, M.; Sehat, A. A.; Dordanihaghighi, S.; Allahbakhsh, A.; van der Kuur, C.; Arjmand, M. Synthesis, Applications, and Prospects of Graphene Quantum Dots: A Comprehensive Review. *Small* **2022**, *18* (2), No. 2102683.

(14) Bacon, M.; Bradley, S. J.; Nann, T. Graphene Quantum Dots. *Part. Part. Syst. Charact.* **2014**, *31* (4), 415−428.

(15) Tian, P.; Tang, L.; Teng, K. S.; Lau, S. P. Graphene Quantum Dots from Chemistry to Applications. *Mater. Today Chem.* **2018**, *10*, 221−258.

(16) Wang, L.; Wang, Y.; Xu, T.; Liao, H.; Yao, C.; Liu, Y.; Li, Z.; Chen, Z.; Pan, D.; Sun, L.; Wu, M. Gram-Scale Synthesis of Single-Crystalline Graphene Quantum Dots with Superior Optical Properties. *Nat. Commun.* **2014**, *5* (1), No. 5357.

(17) Ritter, K. A.; Lyding, J. W. The Influence of Edge Structure on the Electronic Properties of Graphene Quantum Dots and Nanoribbons. *Nat. Mater.* **2009**, *8* (3), 235−242.

(18) Wang, J.; Cao, S.; Ding, Y.; Ma, F.; Lu, W.; Sun, M. Theoretical Investigations of Optical Origins of Fluorescent Graphene Quantum Dots. *Sci. Rep.* **2016**, *6* (1), No. 24850.

(19) Weymann, I.; Barna, J.; Krompiewski, S. Manifestation of the Shape and Edge Effects in Spin-Resolved Transport through Graphene Quantum Dots. *Phys. Rev. B* **2012**, *85* (20), No. 205306.

(20) Ghosh, D.; Sarkar, K.; Devi, P.; Kim, K. H.; Kumar, P. Current and Future Perspectives of Carbon and Graphene Quantum Dots: From Synthesis to Strategy for Building Optoelectronic and Energy Devices. *Renewable Sustainable Energy Rev.* **2021**, *135*, No. 110391.

(21) Ji, Z.; Dervishi, E.; Doorn, S. K.; Sykora, M. Size-Dependent Electronic Properties of Uniform Ensembles of Strongly Confined Graphene Quantum Dots. *J. Phys. Chem. Lett.* **2019**, *10* (5), 953−959.

(22) Ye, R.; Peng, Z.; Metzger, A.; Lin, J.; Mann, J. A.; Huang, K.; Xiang, C.; Fan, X.; Samuel, E. L. G.; Alemany, L. B.; Martí, A. A.; Tour, J. M. Bandgap Engineering of Coal-Derived Graphene Quantum Dots. *ACS Appl. Mater. Interfaces* **2015**, *7* (12), 7041−7048.

(23) Sk, M. A.; Ananthanarayanan, A.; Huang, L.; Lim, K. H.; Chen, P. Revealing the Tunable Photoluminescence Properties of Graphene Quantum Dots. *J. Mater. Chem. C* **2014**, *2* (34), 6954−6960.

(24) Prabhu, S. A.; Kavithayeni, V.; Suganthy, R.; Geetha, K. Graphene Quantum Dots Synthesis and Energy Application: A Review. *Carbon Lett.* **2021**, *31* (1), 1−12.

(25) Sweetman, M. J.; Hickey, S. M.; Brooks, D. A.; Hayball, J. D.; Plush, S. E. A Practical Guide to Prepare and Synthetically Modify Graphene Quantum Dots. *Adv. Funct. Mater.* **2019**, *29* (14), No. 1808740.

(26) Backes, C.; Higgins, T. M.; Kelly, A.; Boland, C.; Harvey, A.; Hanlon, D.; Coleman, J. N. Guidelines for Exfoliation, Characterization and Processing of Layered Materials Produced by Liquid Exfoliation. *Chem. Mater.* **2017**, *29* (1), 243−255.

(27) Coleman, J. N.; Lotya, M.; O'Neill, A.; Bergin, S. D.; King, P. J.; Khan, U.; Young, K.; Gaucher, A.; De, S.; Smith, R. J.; Shvets, I. V.; Arora, S. K.; Stanton, G.; Kim, H. Y.; Lee, K.; Kim, G. T.; Duesberg, G. S.; Hallam, T.; Boland, J. J.; Wang, J. J.; Donegan, J. F.; Grunlan, J. C.; Moriarty, G.; Shmeliov, A.; Nicholls, R. J.; Perkins, J. M.; Grieveson, E. M.; Theuwissen, K.; McComb, D. W.; Nellist, P. D.; Nicolosi, V. Two-Dimensional Nanosheets Produced by Liquid Exfoliation of Layered Materials. *Science* **2011**, *331* (6017), 568−571.

(28) Paton, K. R.; Varrla, E.; Backes, C.; Smith, R. J.; Khan, U.; O'Neill, A.; Boland, C.; Lotya, M.; Istrate, O. M.; King, P.; Higgins, T.; Barwich, S.; May, P.; Puczkarski, P.; Ahmed, I.; Moebius, M.; Pettersson, H.; Long, E.; Coelho, J.; O'Brien, S. E.; McGuire, E. K.; Sanchez, B. M.; Duesberg, G. S.; McEvoy, N.; Pennycook, T. J.; Downing, C.; Crossley, A.; Nicolosi, V.; Coleman, J. N. Scalable Production of Large Quantities of Defect-Free Few-Layer Graphene by Shear Exfoliation in Liquids. *Nat. Mater.* **2014**, *13* (6), 624−630.

(29) Hernandez, Y.; Nicolosi, V.; Lotya, M.; Blighe, F. M.; Sun, Z.; De, S.; McGovern, I. T.; Holland, B.; Byrne, M.; Gun'ko, Y. K.; Boland, J. J.; Niraj, P.; Duesberg, G.; Krishnamurthy, S.; Goodhue, R.; Hutchison, J.; Scardaci, V.; Ferrari, A. C.; Coleman, J. N. High-Yield Production of Graphene by Liquid-Phase Exfoliation of Graphite. *Nat. Nanotechnol.* **2008**, *3* (9), 563−568.

(30) O'Neill, A.; Khan, U.; Nirmalraj, P. N.; Boland, J.; Coleman, J. N. Graphene Dispersion and Exfoliation in Low Boiling Point Solvents. *J. Phys. Chem. C* **2011**, *115* (13), 5422−5428.
(31) Arao, Y.; Kuwahara, R.; Ohno, K.; Tanks, J.; Aida, K.; Kubouchi, M.; Takeda, S. ichi. Mass Production of Low-Boiling Point Solvent- And Water-Soluble Graphene by Simple Salt-Assisted Ball Milling. *Nanoscale Adv.* **2019**, *1* (12), 4955−4964.
(32) Liu, W. W.; Xia, B. Y.; Wang, X. X.; Wang, J. N. Exfoliation and Dispersion of Graphene in Ethanol-Water Mixtures. *Front. Mater. Sci.* **2012**, *6* (2), 176−182.
(33) Tao, H.; Zhang, Y.; Gao, Y.; Sun, Z.; Yan, C.; Texter, J. Scalable Exfoliation and Dispersion of Two-Dimensional Materials-an Update. *Phys. Chem. Chem. Phys.* **2017**, *19* (2), 921−960.
(34) Ghanbari, H.; Shafikhani, M. A.; Daryalaal, M. Graphene Nanosheets Production Using Liquid-Phase Exfoliation of Pre-Milled Graphite in Dimethylformamide and Structural Defects Evaluation. *Ceram. Int.* **2019**, *45* (16), 20051−20057.
(35) Zhao, W.; Fang, M.; Wu, F.; Wu, H.; Wang, L.; Chen, G. Preparation of Graphene by Exfoliation of Graphite Using Wet Ball Milling. *J. Mater. Chem.* **2010**, *20* (28), 5817−5819.
(36) Al-Sherbini, A. S.; Bakr, M.; Ghoneim, I.; Saad, M. Exfoliation of Graphene Sheets via High Energy Wet Milling of Graphite in 2-Ethylhexanol and Kerosene. *J. Adv. Res.* **2017**, *8* (3), 209−215.
(37) León, V.; Quintana, M.; Herrero, M. A.; Fierro, J. L. G.; Hoz, A. D.; Prato, M.; Vázquez, E. Few-Layer Graphenes from Ball-Milling of Graphite with Melamine. *Chem. Commun.* **2011**, *47* (39), 10936−10938.
(38) Knieke, C.; Berger, A.; Voigt, M.; Klupp Taylor, R. N.; Röhrl, J.; Peukert, W. Scalable Production of Graphene Sheets by Mechanical Delamination. *Carbon* **2010**, *48* (11), 3196−3204.
(39) Shang, N. G.; Papakonstantinou, P.; Sharma, S.; Lubarsky, G.; Li, M.; McNeill, D. W.; Quinn, A. J.; Zhou, W.; Blackley, R. Controllable Selective Exfoliation of High-Quality Graphene Nanosheets and Nanodots by Ionic Liquid Assisted Grinding. *Chem. Commun.* **2012**, *48* (13), 1877−1879.
(40) Alinejad, B.; Mahmoodi, K. Synthesis of Graphene Nanoflakes by Grinding Natural Graphite Together with NaCl in a Planetary Ball Mill. *Funct. Mater. Lett.* **2017**, *10* (4), No. 1750047.
(41) González, V. J.; Rodríguez, A. M.; León, V.; Frontiñán-Rubio, J.; Fierro, J. L. G.; Durán-Prado, M.; Muñoz-García, A. B.; Pavone, M.; Vázquez, E. Sweet Graphene: Exfoliation of Graphite and Preparation of Glucose-Graphene Cocrystals through Mechanochemical Treatments. *Green Chem.* **2018**, *20* (15), 3581−3592.
(42) Ciesielski, A.; Haar, S.; Aliprandi, A.; El Garah, M.; Tregnago, G.; Cotella, G. F.; El Gemayel, M.; Richard, F.; Sun, H.; Cacialli, F.; Bonaccorso, F.; Samorì, P. Modifying the Size of Ultrasound-Induced Liquid-Phase Exfoliated Graphene: From Nanosheets to Nanodots. *ACS Nano* **2016**, *10* (12), 10768−10777.
(43) Hadi, A.; Zahirifar, J.; Karimi-Sabet, J.; Dastbaz, A. Graphene Nanosheets Preparation Using Magnetic Nanoparticle Assisted Liquid Phase Exfoliation of Graphite: The Coupled Effect of Ultrasound and Wedging Nanoparticles. *Ultrason. Sonochem.* **2018**, *44*, 204−214.
(44) Zhang, Y.; Li, K.; Ren, S.; Dang, Y.; Liu, G.; Zhang, R.; Zhang, K.; Long, X.; Jia, K. Coal-Derived Graphene Quantum Dots Produced by Ultrasonic Physical Tailoring and Their Capacity for Cu(II) Detection. *ACS Sustainable Chem. Eng.* **2019**, *7* (11), 9793−9799.
(45) Ciesielski, A.; Samorì, P. Graphene via Sonication Assisted Liquid-Phase Exfoliation. *Chem. Soc. Rev.* **2014**, *43* (1), 381−398.
(46) Arao, Y.; Kubouchi, M. High-Rate Production of Few-Layer Graphene by High-Power Probe Sonication. *Carbon* **2015**, *95*, 802−808.
(47) Eda, G.; Lin, Y.; Mattevi, C.; Yamaguchi, H.; Chen, H.; Chen, I.; Chen, C.; Chhowalla, M. Blue Photoluminescence from Chemically Derived Graphene Oxide. *Adv. Mater.* **2010**, *22* (4), 505−509.
(48) Zhu, S.; Tang, S.; Zhang, J.; Yang, B. Control the Size and Surface Chemistry of Graphene for the Rising Fluorescent Materials. *Chem. Commun.* **2012**, *48* (38), 4527−4539.
(49) Monshi, A.; Foroughi, M. R.; Monshi, M. R. Modified Scherrer Equation to Estimate More Accurately Nano-Crystallite Size Using XRD. *World J. Nano Sci. Eng.* **2012**, *02* (03), 154−160.
(50) Zhu, S.; Song, Y.; Wang, J.; Wan, H.; Zhang, Y.; Ning, Y.; Yang, B. Photoluminescence Mechanism in Graphene Quantum Dots: Quantum Confinement Effect and Surface/Edge State. *Nano Today* **2017**, *13*, 10−14.
(51) Liu, Q.; Sun, J.; Gao, K.; Chen, N.; Sun, X.; Ti, D.; Bai, C.; Cui, R.; Qu, L. Graphene Quantum Dots for Energy Storage and Conversion: From Fabrication to Applications. *Mater. Chem. Front.* **2020**, *4* (2), 421−436.
(52) Kwon, W.; Kim, Y.-H.; Kim, J.-H.; Lee, T.; Do, S.; Park, Y.; Jeong, M. S.; Lee, T.-W.; Rhee, S.-W. High Color-Purity Green, Orange, and Red Light-Emitting Diodes Based on Chemically Functionalized Graphene Quantum Dots. *Sci. Rep.* **2016**, *6* (1), No. 24205.
(53) Ferrari, A. C.; Basko, D. M. Raman Spectroscopy as a Versatile Tool for Studying the Properties of Graphene. *Nat. Nanotechnol.* **2013**, *8* (4), 235−246.
(54) Ferrari, A. C.; Robertson, J. Interpretation of Raman Spectra of Disordered and Amorphous Carbon. *Phys. Rev. B* **2000**, *61* (20), 14095−14107.
(55) Cançado, L. G.; Jorio, A.; Ferreira, E. H. M.; Stavale, F.; Achete, C. A.; Capaz, R. B.; Moutinho, M. V. O.; Lombardo, A.; Kulmala, T. S.; Ferrari, A. C. Quantifying Defects in Graphene via Raman Spectroscopy at Different Excitation Energies. *Nano Lett.* **2011**, *11* (8), 3190−3196.
(56) Burikov, S.; Dolenko, T.; Patsaeva, S.; Starokurov, Y.; Yuzhakov, V. Raman and IR Spectroscopy Research on Hydrogen Bonding in Water-Ethanol Systems. *Mol. Phys.* **2010**, *108* (18), 2427−2436.
(57) Alimohammadian, M.; Sohrabi, B. Manipulating Electronic Structure of Graphene for Producing Ferromagnetic Graphene Particles by Leidenfrost Effect-Based Method. *Sci. Rep.* **2020**, *10* (1), No. 6874.
(58) Alimohammadian, M.; Sohrabi, B. Observation of Magnetic Domains in Graphene Magnetized by Controlling Temperature, Strain and Magnetic Field. *Sci. Rep.* **2020**, *10* (1), No. 21325.

https://doi.org/10.1021/acsomega.4c00453
ACS Omega 2024, 9, 31427−31437